ETH zürich

ETH Library

A 4D printed active compliant hinge for potential space applications using shape memory alloys and polymers

Journal Article

Author(s):
Testoni, Oleg; Lumpe, Thomas; Huang, Jian-Lin; Wagner, Marius; Bodkhe, Sampada; Zhakypov, Zhenishbek; Spolenak, Ralph; Paik, Jamie K.; Ermanni, Paolo; Muñoz, Luis; Shea, Kristina

Publication date:
2021-08

Permanent link:
https://doi.org/10.3929/ethz-b-000484678

Rights / license:
In Copyright - Non-Commercial Use Permitted

Originally published in:
Smart Materials and Structures 30(8), https://doi.org/10.1088/1361-665x/ac01fa

This page was generated automatically upon download from the ETH Zurich Research Collection.
For more information, please consult the Terms of use.

A 4D printed active compliant hinge for potential space applications using shape memory alloys and polymers

Oleg Testoni [a,*], Thomas Lumpe [b], Jian-Lin Huang [c], Marius Wagner [d], Sampada Bodkhe [a], Zhenishbek Zhakypov [c], Ralph Spolenak [d], Jamie Paik [c], Paolo Ermanni [a], Luis Muñoz [f] and Kristina Shea [b]

[a] Laboratory of Composite Materials and Adaptive Structures (CMASLab), Department of Mechanical and Process Engineering, ETH Zurich, Leonhardstrasse 21, 8092, Zurich, Switzerland

[b] Engineering Design and Computing Laboratory (EDAC), Department of Mechanical and Process Engineering, ETH Zurich, Tannenstrasse 3, 8092, Zurich, Switzerland

[c] Reconfigurable Robotics Lab (RRL), School of Engineering, EPFL, MED 11326 Station 9, 1015, Lausanne, Switzerland

[d] Laboratory for Nanometallurgy (LNM), Department of Materials, ETH Zurich, Vladimir-Prelog-Weg 5, 8093, Zurich, Switzerland

[e] Orbitare AG, Goldauerstrasse 58, 8006 Zurich, Switzerland

* Corresponding author. E-mail address: testonio@ethz.ch

Abstract

This paper presents the proof-of-concept for a 4D printed active compliant hinge with a selectively variable stiffness for the deployment and reorientation of satellite appendages. We use 4D printing to create an active compliant hinge capable of bending to a given angular position, holding the position without consuming energy and reorienting itself multiple times in a slow and controlled manner without using rigid mechanisms and, therefore, requiring no lubrication. The deployment and the reorientation of the hinge are achieved by exploiting thermally induced stiffness modulation of one of the constituting materials and two antagonistic shape memory alloy actuators. The hinge is specifically designed for the case study of a 6U CubeSat with two orientable solar panels. In this work, we first explain the working principle of the hinge and propose three different actuation strategies to increase the energy collection of the considered CubeSat. Second, we describe the specific functional and geometric requirements of the hinge, the resulting design and the fabricated functional prototype. The latter is tested in a standard laboratory environment to measure the range of motion, the energy consumption and the actuation time. Finally, the feasibility of the three proposed actuation strategies is evaluated considering the corresponding net increase in collected energy. The results show that the hinge is compatible with the stowing requirements and capable of achieving maximum angular positions larger than 90° in both directions and holding any intermediate position with an accuracy of less than 3°. The three actuation strategies considered lead, in a standard laboratory environment, to an increase in energy generation between 54% and 72%.

Keywords

Compliant hinge, 4D printing, selective stiffness, CubeSats, shape memory materials.

1. Introduction

The rapid development of new active materials and the first uses of polymers in space are revolutionizing the space sector. The drive introduced by CubeSats [1] to reduce mission costs through the use of inexpensive components [2] and the simplification of spacecraft designs [3] has prompted many institutions and private companies to consider polymeric materials and novel manufacturing processes, such as 4D printing [4], to devise novel solutions [5]. 4D printing is particularly interesting for the realization of deployable structures without conventional actuators, which can potentially reduce weight and complexity of space systems [6]. The term 4D printing refers to the 3D printing of objects capable of changing their properties, such as shape or stiffness, when subject to external stimuli, such as heat, UV light or humidity [7].

Shape memory polymers (SMPs) are a class of 4D printable materials reacting to a thermal stimulus by changing their elastic modulus of several orders of magnitude [8] and are particularly promising for space applications due to their low density, low cost, high shape deformability and easily tailorable glass transition temperature [9]. These unique properties make SMPs suitable for the realization of complaint systems for the deployment and the reorientation of satellite appendages [9]. Despite the challenge of using polymers in space identified by various studies [10-16], several research groups have proposed the use of SMPs and their composites for space applications, such as deployable booms [17], reconfigurable antennas [18] and compliant hinges [19-21].

Compared to more traditional hinge designs based on revolute joints or on more complex mechanisms [22-26], compliant hinges have the advantage of requiring no lubrication and having no risk of galling and cold welding in space [27]. Yet, most types of compliant hinges are based on tape springs and are characterized by a rapid deployment, which might lead to high locking shocks or even collisions with other satellite appendages [28-31]. Alternative solutions relying on shape memory alloys (SMAs) [32-34] and shape memory polymers [35-36] have been proposed to achieve a slow and controlled deployment. However, all the compliant hinge designs found in the literature cannot be actuated multiple times and, therefore, are suitable only for one-time deployment and not for the reorientation of appendages [7, 37].

In this paper, we contribute to the work on compliant hinges for space applications proposing the concept of a 4D-printed active complaint hinge with selectively variable stiffness combining shape memory polymers and alloys to achieve multiple and repeatable actuations. The hinge is suitable for both the deployment and the reorientation of satellite appendages and is capable of holding a given angular position without consuming energy. The design of the hinge is developed considering the case study of a 6U CubeSat with two orientable solar panels. As proof-of-concept, a functional prototype is built, tested, and its energy consumption and actuation time are measured under standard laboratory conditions to verify the compatibility with the considered CubeSat platform.

2. Method

2.1 Case study

The design of the proposed hinge concept is developed considering the case of a 6U CubeSat with two orientable solar panels as depicted in Fig. 1. Each solar panel has solar cells only on the upper side and is connected to the main body of the satellite by two active compliant hinges on the longest edge. The hinges must be capable of bending to angular positions between 90° on both sides of the hinge for the stowing of the satellite in a dispenser (Fig. 1-a), the deployment of the panels after the ejection of the satellite (Fig. 1-b), and their reorientation in

any desired direction (Fig. 1-c and 1-d). Due to microgravity conditions, loads from the solar panels have no influence on the bending angle achieved by the hinge and are not considered.

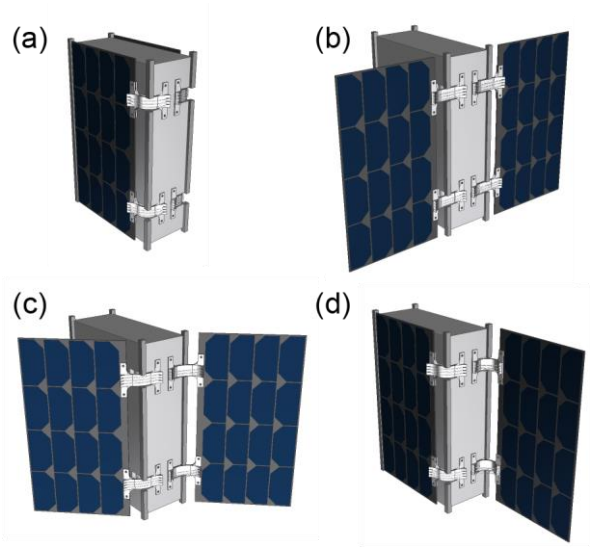

Figure 1: Case study: (a) stowed satellite, (b) fully deployed panels (reference position), (c) panels oriented at 45° and (d) panels oriented at 90°.

In order to show the potential benefit of the proposed hinge concept, we consider three different actuation strategies of the hinge and calculate the corresponding theoretical increase in energy collection per orbit compared to a reference satellite configuration with fixed panels oriented perpendicularly to the local vertical (see Fig. 2). This calculation is carried out considering a sun-synchronous Low Earth Orbit (LEO) with 40% of the orbital period in eclipse and neglecting the effect of penumbra and albedo. Moreover, we assume that the panels are always parallel to each other along the orbit and, therefore, oriented with the same angle with respect to the sun.

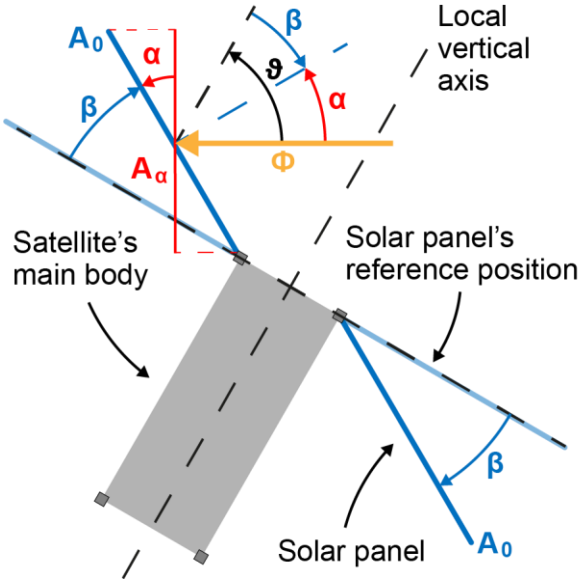

Figure 2: Orientation of the satellite ϑ and of its panels α with respect to the incoming solar flux *Φ*. β angular positon of the solar panels with respect to the reference positon.

Referring to Fig. 2, we define *ϑ* as the angle between the direction of the solar flux *Φ* and the local vertical axis of the satellite, *β* the orientation of the panels with respect to their reference position, corresponding to the angle between the normal to the panels' surface and the local

vertical axis, and α the angle of incidence of the solar flux on the panels. α depends on the position of the satellite along the orbit and on the orientation of the panels:

$$\alpha = \vartheta - \beta \tag{1}$$

Assuming that the solar cells installed on the panels have an area A and an efficiency ε, independent of the inclination angle α, the power collected by the satellite W can be expressed as:

$$W_{(\vartheta,\beta)} = \Phi \cdot \varepsilon \cdot A \cdot \cos \alpha_{(\vartheta,\beta)} \tag{2}$$

The energy collected per orbit E is the integral of the power collected over the orbital period T and, considering a circular orbit, it can be expressed as:

$$E = \int_T W_{(\vartheta,\beta)} dt = \int_0^{2\pi} W_{(\vartheta,\beta)} \frac{T}{2\pi} d\vartheta \tag{3}$$

since the angular speed is constant and equal to:

$$\dot{\vartheta} = \frac{d\vartheta}{dt} = \frac{2\pi}{T} \tag{4}$$

E is a function of the orientation of the panels β and can be increased by using the active hinges to adjust the value of β along the satellite's orbit (see Fig. 3). E is maximized when the panels are always perpendicular to the solar flux ($\alpha = 0$). This condition is achieved by applying a sun-tracking actuation strategy of the hinges to constantly reorient the panels so that $\beta = \vartheta$. However, the constant reorientation of the panels implies the constant powering of the hinges. Therefore, even if the energy collection is maximized, this actuation strategy might not be the most energy efficient. For this reason, we consider also two other actuation strategies, in which the panels are reoriented in three and five discrete steps, respectively, in order to reduce the energy consumption of the hinges by activating them only for the time necessary to rotate the panels of a given angle. Fig. 3 depicts the potential benefit of the active compliant hinges comparing the energy collection along the considered orbit in the case of fixed solar panels (Fig. 3-a), sun-tracking panels (Fig. 3-b), as well as three- and five-step actuation (Fig. 3-c and 3-d, respectively). The detailed calculation of the energy collected by the different strategies is reported in the Appendix.

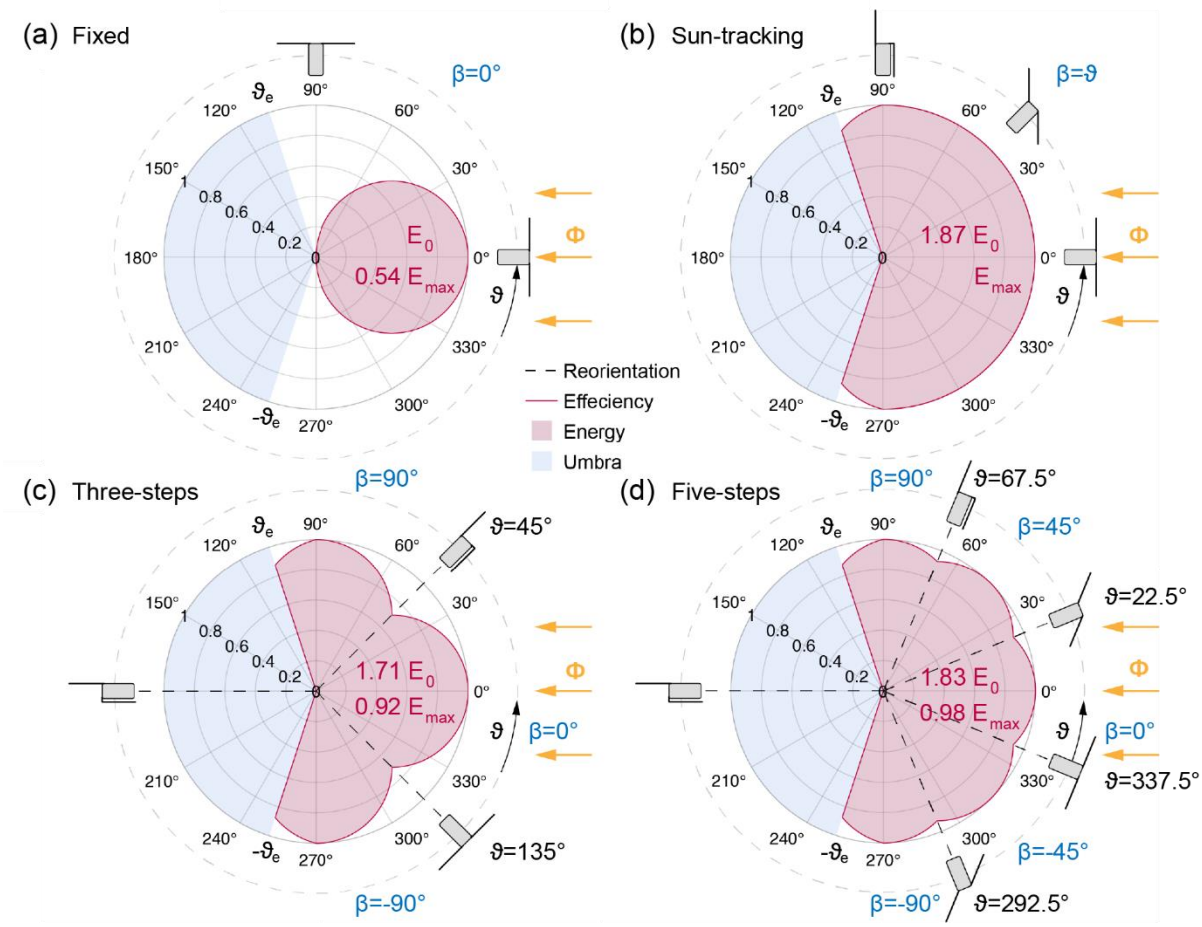

Figure 3: Schematic representation of the actuation strategies of the active complaint hinges and of the corresponding orientation of the solar panels along the orbit of the satellite: (a) fixed panels, (b) sun-tracking panels, (c) three-step actuation and (d) five-step actuation.

2.2 Approach and working principle

We take advantage of the combination of SMPs and SMAs to create the proof-of-concept of an active compliant hinge with selectively variable bending stiffness combining the simplicity of a compliant hinge with the reorientation capability of more complex, rigid mechanisms. Moreover, we use the PolyJet process [38] to realize multi-material 3D printed components made of two different SMPs with different glass transition temperatures (T_g). This process limits the selective reduction in stiffness to only the central region of the hinge and preserves the original stiffness in the regions used to attach the SMAs and to connect the hinge to the main body of the satellite and to the solar panels. The SMPs used are VeroWhite+ (VW+) [39] and High Temperature polymer (HT) [40], which are characterized by a T_g of 53°C and 64°C, respectively.

The variation in bending stiffness is achieved by applying a thermal input to heat the central region of the hinge above the T_g of VW+. The resulting reduction in Young's modulus of the SMP leads to a temporary increase in compliance and enables the bending of the hinge through a SMA spring (Fig. 4). The change in stiffness allows the hinge to achieve large angular positions with little actuation force and to hold any angular position in its range of motion without consuming energy. This effect is achieved by keeping the hinge in the desired position using the SMA springs, while letting the hinge cool down below the T_g to restore the initial stiffness. Once the initial stiffness is restored, the hinge is frozen in a deformed state and can hold the angular position without powering the SMAs. Finally, the reheating above the T_g enables the recovery of the original shape and thus allows for multiple actuations of the hinge.

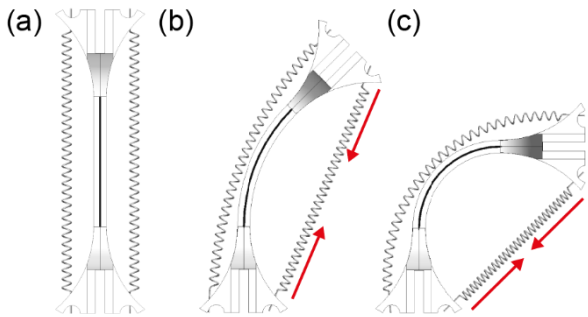

Figure 4: Actuation of the active compliant hinge: (a) initial configuration, (b) hinge bent at 45° and (c) hinge bent at 90°.

The hinge design presented in this work is developed to satisfy a series of basic geometrical and functional requirements. The hinge is sized to be sufficiently compact to enable its installation on a 6U CubeSat and the stowing of the satellite in a dispenser. Two resistive heaters are embedded in the hinge to control the stiffness. The materials and the layup of the components are selected to allow the hinge to achieve large angular positons multiple times in positive and negative direction without undergoing mechanical failure. Finally, the SMA springs are dimensioned to achieve sufficiently high forces and strokes to bend the hinge to 90°.

2.3 Experimental characterization

A functional prototype of the hinge is built and tested to demonstrate the feasibility of the concept for the deployment and the reorientation of satellite appendages. All tests are performed in a laboratory environment at standard temperature and pressure. One end of the prototype is fixed to a vertical support and the angular position β of the other end is measured using a camera and the software Tracker. The SMA springs are actuated with a current i_{SMA}, which is varied between 0 and 1 A, and have a maximum power consumption of 2.5 W each at i_{SMA} = 1 A. The heaters are powered with a constant current i_h = 0.3 A and consume 0.75 W each. SMA springs and heaters are controlled via a microcontroller (Arduino Mega) and power electronics. A LabView interface is used to implement a closed-loop control system, which adjusts the values of i_{SMA} and i_h using a camera to measure the angular position of the hinge. The microcontroller receives the command and generates the pulse-width modulation (PWM) with adjusted duty cycles for regulating the input power to actuators and heaters (Fig. 5-b). The power electronics consist of a DC power supply (RND 320-KD3005P, RDN LAB) and transistor switches. The PWM signal is sent to the transistors to regulate the power level proportionally to the duty value. The detailed electronics setup is described in [41]. Additionally, a thermal imaging temperature sensor (FLIR A35, FLIR Systems Inc.) is used for monitoring the temperature of the different components.

A series of tests is carried out to investigate the performance of the prototype in terms of range of motion, energy consumption and actuation time. In each test, the heaters are turned on and powered for 180 s before the start of the measurements.

Bending and locking at maximum angular position

The maximum angular position β_{max} at which the hinge can be locked is measured. A SMA spring is actuated increasing gradually the value of i_{SMA} to 1 A. After 120 s, the heaters are turned off while keeping powering the SMA spring with i_{SMA} = 1 A for other 180 s until the prototype has recovered the initial stiffness. Finally, the SMA spring is turned off and the value of β_{max} is measured. After 420 s from the start of the measurement, the heaters are turned on again to measure the capability to the prototype of recovering the initial angular position of 0° when only the heaters are powered.

Multiple actuation
The possibility to actuate the hinge multiple times in a repeatable manner is investigated. The prototype is bent at its maximum angular position for five consecutive cycles with a period of 180 s. In each cycle, the prototype is bent in both positive and negative direction actuating the SMA springs as follows: i_{SMA} is gradually increased from 0 to 1 A in 30 s, kept at 1 A for other 30 s and then turned off. After other 30 s, the opposite SMA spring is actuated and the same process is repeated in the other direction.

Gradual increase in angular position
The possibility to precisely control the hinge by actuating a single SMA spring is investigated. The controller tunes the value of i_{SMA} to vary the angular position β of the prototype from 0° to 90° in steps of 10°.

Multi-step actuation
The possibility to actuate the hinge in multiple steps coordinating both SMA springs to implement the suggested actuation strategies is investigated. The control algorithm adjusts the values of i_{SMA} to bend the hinge at the following angular positions: 45°, 90°, -90° and 45°. Moreover, at each angular position, the power consumed by the prototype to hold its position is measured and used in the estimation of the energy consumption.

2.4 Estimation of energy performance and actuation time

The feasibility of the three actuation strategies described in section 2.1 is assessed by estimating the theoretical net increase in energy collection and by comparing the actuation time of the prototype with the allowable time. The energy collected by the reference satellite configuration E_0 and the allowable actuation times of the hinge are calculated assuming a total payload power W_{pl} = 20 W [42] and an orbital altitude h = 600 km. The orbital period T is calculated using the following formula [43]:

$$T = 2\pi\sqrt{\frac{(h + r_E)^3}{GM}} \tag{5}$$

where r_E is the average radius of Earth, equal to 6’378 km, and GM is the standard gravitational parameter of Earth, equal to 398’600 km^{3}s^{-2} [44].

In order to keep a constant energy balance, the energy E_0 collected by the reference satellite in each orbit has to be equal to energy consumed by the satellite’s systems:

$$E_0 = TW_{pl} \tag{6}$$

E_0 is the reference value used for the estimation of the energy collection of the considered actuation strategies described in Fig. 2 and in the Appendix. Finally, for each actuation strategy, the net increase in energy collection is calculated subtracting the relative energy consumption of four hinges from the energy collected.

The energy consumption of a hinge is calculated summing the energy consumption of the heaters and the SMA springs. At each step of the three- and five-step actuation strategies, the heaters are powered with 1.5 W for 300 s: 180 s before and 120 s after the actuation of the SMA spring. The latter is also actuated for 300 s and its energy consumption is based on the power required to hold the hinge at ±45° or ±90° measured in the multi-step actuation test. In the sun-tracking actuation strategy, the heaters are assumed to be powered with 1.5 W during the entire full-light phase of the satellite and for 180 s during the eclipse phase. A SMA spring is assumed to be constantly actuated during the entire full-light phase and for 300 s in the

eclipse phase. The power required by the SMA springs is based on the power required to hold the hinge 90° measured in the multi-step actuation test.

The allowable actuation times of the hinges is obtained by considering the time in full-light T_S of the satellite. Since the satellite is in eclipse for 40% of its orbit, T_S amounts to 60% of the orbital period (T_S = 0.6 T). The allowable actuation times for the three- and for five-step actuation strategies are calculated by dividing T_S by a factor two and a factor four, respectively, since the three-step strategy requires two actuation steps in the full-light region, while the five-step strategy four steps.

3. Results

3.1 Hinge design

The design of the hinge developed in this work is depicted in Fig. 5 and has a size of approximately 70 x 60 x 21 mm^3. It consists of two identical, 3D printed, multi-material SMP parts, separated by a central layer of unidirectional carbon fiber reinforced polymer (CFRP), and actuated by two antagonistic Nickel-Titanium SMA springs. The two multi-material parts are characterized by an outer region in HT and an inner region in VW+, highlighted in yellow in Fig. 5-b. The outer region has a higher T_g and hosts shanks for the attachment of the SMA springs and holes for fixing the hinge to the main body of the satellite and to the solar panels. The inner region has a size of 30 x 20 x 1.3 mm^3 and is characterized by a lower T_g. Two heaters are embedded between the inner region and the CFRP layer to control the temperature and selectively vary the stiffness of the hinge. Each heater consists of a thin copper film with a serpentine path, which provides a high electrical resistance but also a high mechanical compliance in order to accommodate large deformations. The CFRP layer has a thickness of 0.1 mm and fibers aligned with the longitudinal axis of the hinge. This layer lays on the neutral axis of the hinge and supports the 3D printed parts at large angular positions, preventing large localized deformations at the center of the hinge, which would lead to mechanical failure, and returning a homogeneous curvature over the entire length of the hinge.

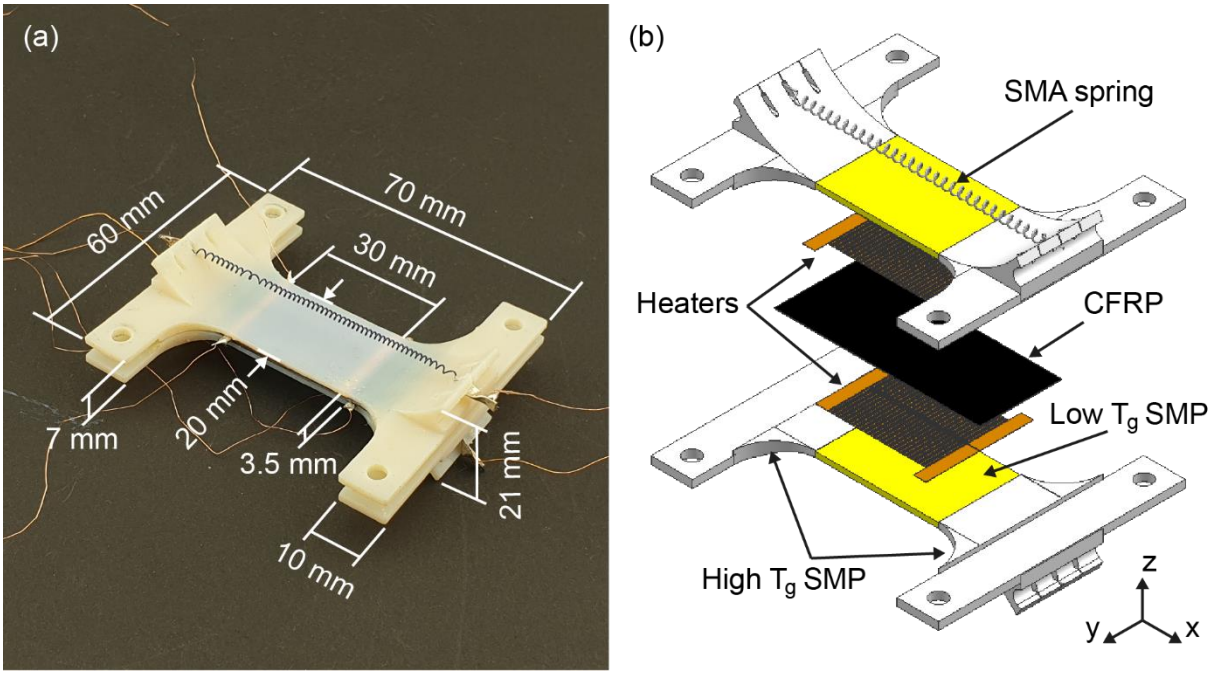

Figure 5: (a) Functional prototype and (b) exploded view of the active compliant hinge. The region of the hinge with selectively variable stiffness is marked in yellow.

A combined manufacturing approach of multi-material 3D printing and manual assembly is used for the fabrication of a functional prototype. The multi-material parts are printed on a

Stratasys Connex3 Objet500 inkjet 3D printer with a matte surface option. The resistive heaters are manufactured by laser cutting (LAB 3550, Inno6 Inc.) a 50 µm thick copper-polyimide film (Pyralux AP, DuPont). Copper wires are soldered on tiny flaps on the side of the heaters for electrical connections. The CFRP layer is fabricated by laying a single ply of unidirectional carbon fiber epoxy prepreg (TC250/HTS40-12K/150, Toray) between two aluminum plates and curing under vacuum for 2 hours at 130°C and 6 bars. The SMA spring actuators are fabricated according to the process described in [45]: commercial NiTi wires with 380 µm diameter (Dynalloy Inc.) are cut, wound around a mandrel of 1.6 mm diameter and annealed at 405 °C for 30 minutes. The prototype is assembled by joining the 3D printed parts, the heaters and the CFRP layer with a flexible adhesive (Cementit Flex, merz+benteli) and by pressing them together with a weight of 1 kg. After for 24 hours, the weight is removed and the excessive glue pouring out from the side of the hinge removed mechanically. Finally, a SMA spring is inserted in the central shanks on each side of the prototype and fixed using crimps.

3.2 Experimental results

Bending and locking at maximum angular position

Fig. 6-a reports the angular position of the prototype as well as the values of i_{SMA} and i_h starting from the actuation of the SMA spring. During the actuation, the prototype reaches a maximum angular position of approximately 97°. After the deactivation of the SMA spring, the prototype recovers parts of the deformation and stabilizes at an angular position of 90°. As a result, considering also the 180 s required to heat up the hinge, the prototype required about 500 s to lock at the maximum angular position. Finally, starting from this position, the prototype recovers an angular position of about 11° in 320 s (Fig. 7-a).

Multiple actuation

Fig. 6-b illustrates the angular positon of the prototype and the input currents of the two antagonistic SMA springs during the multiple actuation test. The results show that the prototype reaches a maximum angular positon of 96° in the first actuation and of about ±100° in following actuations (Fig. 7-b).

Gradual increase in angular position

Fig. 6-c shows the gradual increase in angular position of the prototype from 0° to 90°. The results show that the prototype can achieve the target angular positions with an accuracy of ±3° over the entire range of angular positions considered.

Multi-step actuation

Fig. 6-d shows the angular position of the prototype in the multi-step actuation test. The results show that the prototype can achieve the target angular positions of ±45° within an actuation time of 30 s when starting from an angular position of 0° and -90°, respectively. On the other hand, the plot shows that the control algorithm takes about 120 s to bend to the prototype at the maximum angular positions of ±90° and to move from -45° to +45° (Fig. 7-c). The power required by the SMA springs to hold the prototype at an angular position of ±45° and ±90° amounts to 0.25 W and 1 W, respectively.

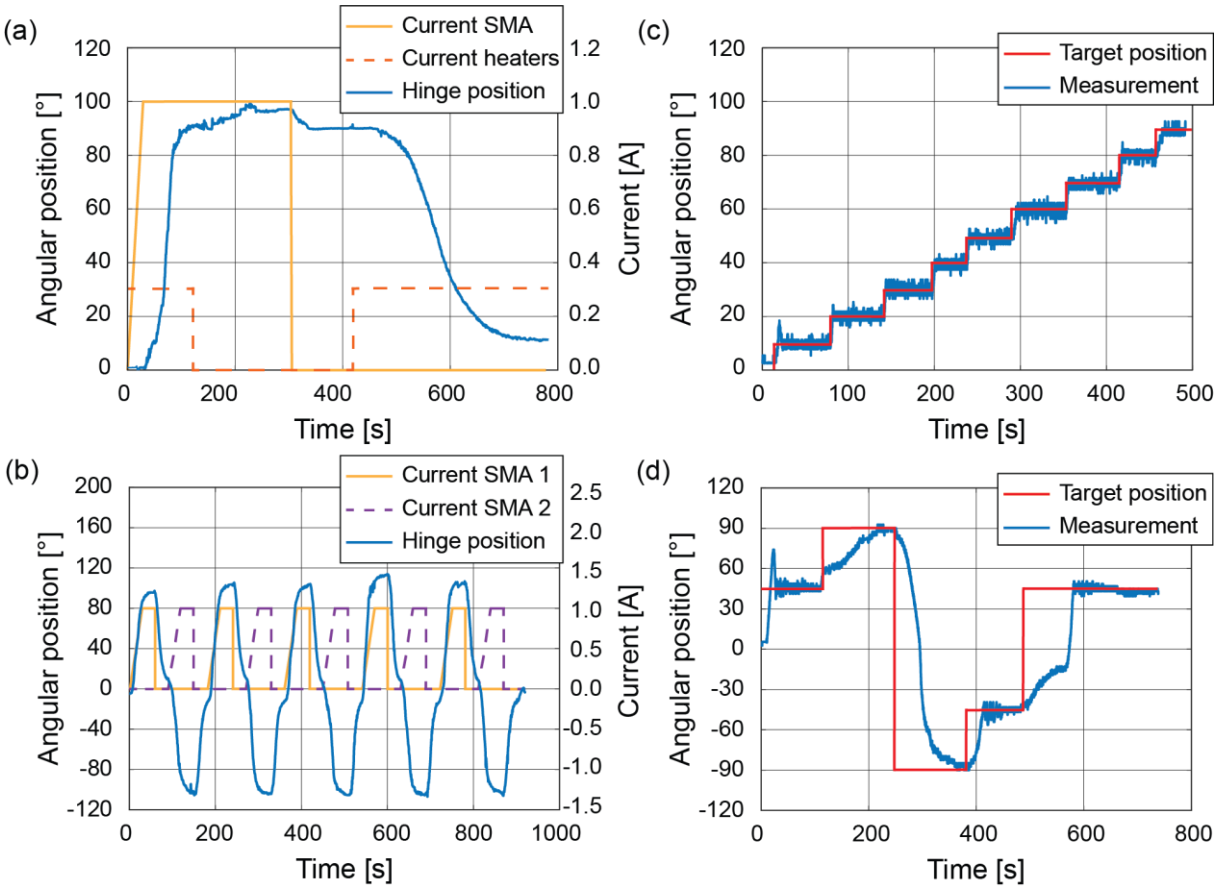

Figure 6: (a) Bending and locking at maximum angular position, (b) multiple actuation, (c) gradual increase in angular position and (d) multi-step actuation.

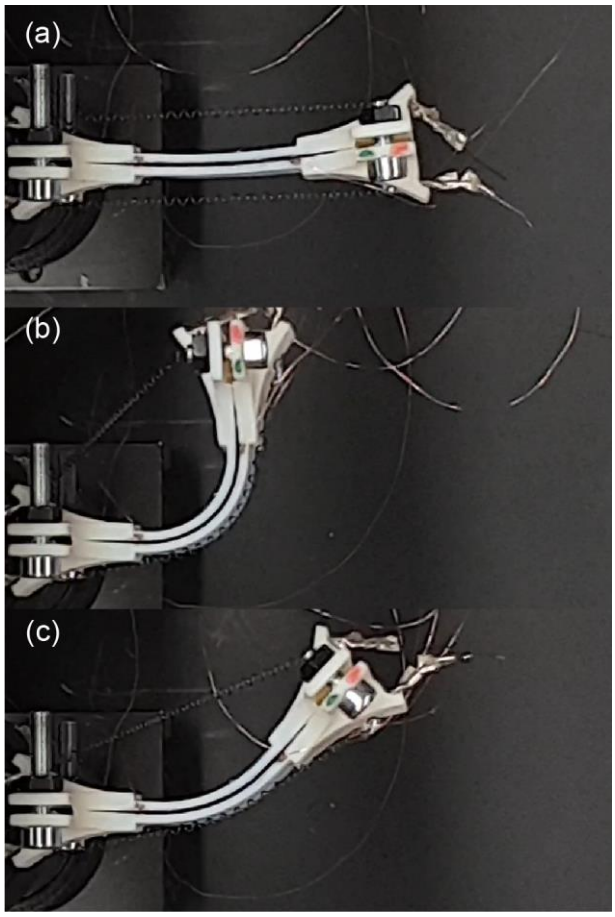

Figure 7: (a) Deployment from the stowed configuration, (b) bending at the maximum angular position and (c) locking at a target angular position of 45°.

3.3 Estimation of energy performance and actuation time

The orbital period calculated with Eq. 5 amounts to T = 5801 s, with a corresponding full-light exposure time T_S = 3481 s, and an energy collected per orbit E_0 = 116 kJ. The energy collected by the proposed actuation strategies is reported in Table 1.

In a single actuation step, the heaters consume 450 J (2 · 0.75 W · 300 s), while the SMA springs 75 J (0.25 W · 300 s) or 300 J (1 W · 300 s) according to the target angular position of ±45° and ±90°, respectively. Considering all four hinges, the satellite requires 2.1 kJ and 3.0 kJ to reorient the panels at ±45° and ±90°, respectively. Therefore, the total energy consumption of the three- and of the five-step actuation strategy amounts to 9.0 kJ and 13.2 kJ, respectively. In the case of sun-tracking actuation, the heaters and the SMA springs require respectively 5.22 kJ (2 · 0.75 W · 3481 s) and 3.48 kJ (1 W · 3481 s) in full-light. Considering four hinges, the energy required in full-light amounts to 34.8 kJ. By adding the 3.0 kJ required in eclipse to reorient the panels, the total energy consumption of the sun-tracking actuation strategy amounts to 37.8 kJ.

The maximum allowable actuation time to implement the three- and the five-step actuation strategy amounts to 1’740 s and 870 s, respectively, while the time required by a single step is 500 s: 180 s to heat up the hinge, and 320 s to bend and lock the hinge.

Table 1: Energy collected, energy consumed, net energy gain and allowable actuation time for the considered actuation strategies. The net energy gain is calculated with respect to a satellite configuration with fixed panels.

	Collected energy	**Consumed energy**	**Net energy gain**	**Allowable actuation time**
Fixed	116 kJ	0 kJ	0 kJ (+ 0%)	-
Sun-tracking	217 kJ	37.8 kJ	63.2 kJ (+ 54%)	-
Three steps	198.5 kJ	9.0 kJ	73.5 kJ (+63 %)	1740 s
Five steps	212.5 kJ	13.2 kJ	83.3 kJ (+72%)	870 s

4. Discussion

4.1 Approach and proof-of-concept

The results obtained demonstrate that 4D printing is a suitable method for the realization of an active compliant hinge that, combining active materials and 3D printing, shows a unique palette of properties, such as compliance, variable stiffness and multiple actuation, not achievable by any other type of hinge. Our approach based on the combination of SMPs and SMAs allows for the realization of an active compliant hinge capable of varying its bending stiffness to achieve angular positons larger than 90° in both directions and to hold any target position in its range of motion without consuming energy. Moreover, the 3D printing of multi-material components and the used of embedded heaters enable the implementation of thermally induced stiffness modulation without compromising the mechanical properties of the components of the hinge and of the adhesive used to join them.

The tests performed demonstrate also the feasibility of our hinge concept to be deployed and reoriented multiple times. On one hand, the functional prototype is capable of holding an angular position of 90° for stowing without consuming energy and of deploying to a neutral position of 0° if the SMA spring under tension is actuated. In addition, even if only the heaters are powered, the prototype is still capable of deploying and recovering almost 80°, returning a feature that might be useful to reorient the hinge towards the neutral position in case of failure of the actuation system. On the other hand, the prototype shows a predictable and repeatable behavior and it is capable of reorient itself in different angular positions multiple times in a controlled manner and with a precision of 3°.

4.2 Energy balance and actuation strategies

The tests carried out on the prototype show that, under standard temperature and pressure conditions, the actuation speed and the energy consumption of the hinge are compatible with all proposed actuation strategies. The time necessary to reorient and lock the hinge in a new angular positon is 500 s. This value is lower than the 870 s required by the five-step actuation strategy, which is the most demanding among the strategies proposed. In addition, the actuation time might be further reduced by monitoring the temperature of the hinge and optimizing the actuation accordingly.

The energy requirements of the three- and of the five-step actuation strategy are about eight and six times lower than the corresponding gain in energy collection theoretically achievable. If compared with the reference satellite configuration with fixed panel, these two actuation strategies lead to a net increase in energy collected of about 63% and 72%, respectively. On the other hand, the sun-tracking actuation strategy has a power consumption only 1.7 times lower than the increase in energy collection and a gain with respect to the reference

configuration of 54%. However, the power consumption of this actuation strategy might be overestimated since it is assumed that heaters and SMA springs are always activated at a constant power when the satellite is in full-light. In reality, this condition might not be necessary and the power consumption of heaters and SMA springs might be reduced. Therefore, the increase in energy collection calculated represents the minimum value achievable under standard temperature and pressure conditions.

4.3 Space readiness

The LEO is characterized by various environmental factors, such as atomic oxygen, UV and ionizing radiation, high vacuum, plasma, micrometeoroids, and cycling temperature that have severe detrimental effects on the properties of polymers and of their composites [10-16]. Different solutions can be applied to reduce the negative effects of these factors, such as the use of protective coatings [46-48] and active shields [49-50]. Addressing these challenges is outside the scope of this study. However, we are aware that these factors may limit the functioning of the hinge and restrict its operative life. Therefore, further studies are needed in order to investigate the effects of the space environment of the behaviour of hinge and on the properties of its components.

Particularly relevant is the effect of high vacuum and large temperature variations on the actuation time and energy consumption of the hinge. In vacuum, no heat can be transferred via convection. Therefore, the cooling of the hinge has to rely only on conduction and radiation. Moreover, sudden changes in temperature may lead to unwanted actuations or locking of the hinge. For these reasons, a suitable thermal management system is needed to regulate the temperature of the hinge. This is a standard and well-established procedure in space systems and relies on passive and active systems, such as thermal coatings, sunshields, thermal straps, radiators and heaters, to regulate the temperature of critical components and to dissipate the excessive heat towards the outer space [51-52].

As a result, we expect the energy consumption and the actuation time to vary from what is measured in laboratory. However, in order to draw definitive conclusions about the energy consumption, the thermal management of the entire satellite should be considered. Indeed, the hinge already has two integrated heaters, whose heat might be funneled elsewhere in the satellite after actuation and be used to heat other components. Therefore, further studies are needed to investigate the effects of vacuum and large variations in temperature on the hinge. In this work, we have demonstrated the feasibility of the proposed hinge concept under standard conditions and found no intrinsic reason to exclude the functioning of the hinge in space.

5. Conclusions

Exploiting the combination of SMPs and SMAs, a novel design for an active compliant hinge with selectively variable bending stiffness is presented that combines the simplicity of a compliant hinge with the reorientation capability of a more complex, rigid mechanism. The hinge meets the stowing requirement of the considered case study of a 6U CubeSat with orientable solar panels, is capable of being actuated multiple times in a slow and controlled manner and can hold any angular position between -90° and + 90° with a precision of 3° without consuming energy. In addition, we propose three different actuation strategies for the hinge to increase the energy collection and demonstrate that, in standard laboratory environment, they lead to a net increase in collected energy between 54% and 72% with respect to a satellite with fixed solar panels.

This work demonstrates that merging the 4D printing of SMPs and SMA actuators is suitable for the creation of active compliant hinges with a unique combination of properties, which may be capable of significantly increasing the energy collection in small satellites without adding

mechanical complexity. The proposed hinge provides the base design for a simple solution to expand the range of applications of CubeSat platforms by allowing for a substantial increase in payload power. Moreover, we believe that the same approach can be extended to other types of space structures, such as booms or antennas, to realize low-energy and tailor-made adaptive systems. Further work should focus on evaluating the actuation time and the energy consumption of the hinge in vacuum, investigate the effects of the space environment on the hinge and on the mechanical properties of its components and assess the expected operative life.

Acknowledgments

This work was supported by the Strategic Focus Area Advanced Manufacturing of the ETH Board through the project “Sustainable Design of 4D Printed Active Systems”.

References

1- J. Puig-Suari, C. Turner, R.J. Twiggs, CubeSat: The Development and Launch Support Infrastructure for Eighteen Different Satellite Customers on One Launch, AIAA/USU Conference on Small Satellites, 2001.
2- K. Woellert, P. Ehrenfreund, A.J. Ricco, H. Hertzfeld, Cubesats: Cost-effective science and technology platforms for emerging and developing nations, Advances in Space Research 47 (2011) 663–684.
3- National Aeronautics and Space Administration, CubeSat 101 Basic Concepts and Processes for First-Time CubeSat Developers. https://www.nasa.gov/sites/default/files/atoms/files/nasa_csli_cubesat_101_508.pdf, 2017 (accessed 10 January 2020).
4- Tibbits, S. (2014), 4D Printing: Multi-Material Shape Change. Archit Design, 84: 116-121. https://doi.org/10.1002/ad.1710
5- Farhang Momeni, Seyed M.Mehdi Hassani.N, Xun Liu, Jun Ni, A review of 4D printing, Materials & Design, Volume 122, 2017, 42-79, https://doi.org/10.1016/j.matdes.2017.02.068.
6- T. Chen, O. R. Bilal, R. Lang, C. Daraio, K. Shea, Autonomous Deployment of a Solar Panel Using Elastic Origami and Distributed Shape-Memory-Polymer Actuators, Physical Review Applied 11, 064069 (2019).
7- A. Mitchell, U. Lafont, M. Hołyńska, C. Semprimoschnig, Additive manufacturing — A review of 4D printing and future applications, Additive Manufacturing 24 (2018) 606–626.
8- McClung A J W, Tandon G P and Baur J W 2012 Strain rate and temperature-dependent tensile properties of an epoxy-based, thermosetting, shape memory polymer Mech. Time-Dep. Mater. 16 205–21.
9- Y. Liu, H. Du, L. Liu, J. Leng, Shape memory polymers and their composites in aerospace applications: a review, Smart Mater. Struct. 23 (2014) 023001 (22pp).
10- Awaja, Firas, et al. "Surface molecular degradation of 3D glass polymer composite under low earth orbit simulated space environment." Polymer Degradation and Stability 95.6 (2010): 987-996.
11- Grossman, E., and I. Gouzman. "Space environment effects on polymers in low earth orbit." Nuclear Instruments and Methods in Physics Research Section B: Beam Interactions with Materials and Atoms 208 (2003): 48-57.
12- Awaja, Firas, et al. "Surface molecular degradation of selected high performance polymer composites under low earth orbit environmental conditions." Polymer degradation and stability 96.7 (2011): 1301-1309.
13- Han, Joo-Hyun, and Chun-Gon Kim. "Low earth orbit space environment simulation and its effects on graphite/epoxy composites." Composite structures 72.2 (2006): 218-226.

14- Chen, Jun, et al. "Organic polymer materials in the space environment." Progress in Aerospace Sciences 83 (2016): 37-56.
15- Park, Sang Yoon, et al. "Effect of vacuum thermal cyclic exposures on unidirectional carbon fiber/epoxy composites for low earth orbit space applications." Composites Part B: Engineering 43.2 (2012): 726-738.
16- Fulcher, J. T., et al. "Thermomechanical characterization of environmentally conditioned shape memory polymer using nanoindentation." Behavior and Mechanics of Multifunctional Materials and Composites 2010. Vol. 7644. International Society for Optics and Photonics, 2010.
17- Jin-Ho Roh, Hye-Jung Kim and Jae-Sung Bae, Shape memory polymer composites with woven fabric reinforcement for self-deployable booms, Journal of Intelligent Material Systems and Structures2014, Vol. 25(18) 2256–2266, DOI: 10.1177/1045389X14544148
18- Santo, Loredana, Fabrizio Quadrini, and Denise Bellisario. "Shape memory composite antennas for space applications." Mater Sci Eng 161.1 (2016): 012066.
19- Chen, Qiaofeng, et al. "Design and testing of a space deployable mechanism." 4th AIAA spacecraft structures conference. 2017.
20- Rakow, Alexi, Kevin Hedin, and Brian Anthony. "Development of high specific power solar arrays with shape memory polymer hinge lines." 2018 AIAA Spacecraft Structures Conference. 2018.
21- Liu, Tianzhen, et al. "Integrative hinge based on shape memory polymer composites: material, design, properties and application." Composite Structures 206 (2018): 164-176.
22- F. Santoni, F. Piergentili, S. Donati, M. Perellic, A. Negric, M. Marino, An innovative deployable solar panel system for Cubesats, Acta Astronautica 95 (2014) 210–217.
23- F. Santoni, F. Piergentili, G. Candini, M. Perelli, A. Negri, M. Marino, An orientable solar panel system for nanospacecraft, Acta Astronautica 101 (2014) 120–128.
24- A. Solís-Santomé, G. Urriolagoitia-Sosa, B. Romero-Ángeles, C.R. Torres-San Miguel, J.J. Hernández-Gómez, I. Medina-Sánchez, C. Couder-Castañeda, J.I. Grageda-Arellano, G. Urriolagoitia-Calderón, Conceptual design and finite element method validation of a new type of self-locking hinge for deployable CubeSat solar panels, Advances in Mechanical Engineering2019, Vol. 11(1) 1–13.
25- J.M. Plaza, J.A. Vilan, F.A. Agelet, J.B. Mancheno, M.L. Estevez, C.M. Fernandez, F.S. Ares, Xatcobeo: small mechanisms for Cubesat satellites antenna and solar array deployment, Proceedings of the 40th Aerospace Mechanisms Symposium, NASA Kennedy Space Centre, May 12–14, 2010, p. 415–429.
26- P. Senatore, A. Klesh, T. H. Zurbuchen, D. McKauge, J. Cutler, Concept, design and prototyping of XSAS: a high power extendable solar array for CubeSat applications, Proceedings of the 40th Aerospace Mechanisms Symposium, NASA Kennedy Space Centre, May 12-14, 2010, p.431–444.
27- J. Fontaine, Towards the use of diamond-like carbon solid lubricant coatings in vacuum and space environments, Proc. IMechE Vol. 222 Part J: J. Engineering Tribology.
28- Ö. Soykasap, Analysis of tape spring hinges, International Journal of Mechanical Sciences 49 (2007) 853–860.
29- E. Ziade, C.S. Patmont, T.A. Fritz, Design and Characterization of a Spring Steel Hinge for Deployable CubeSat Structures, JoSS, Vol. 5, No. 1 (2016), pp. 407–418.
30- J. Sincre, D. Givois, A. Emerit, Application of “Maeva Hinge To Myriade Microsatellites, Proceedings of the 11th European Space Mechanisms and Tribology Symposium, ESMATS 2005, 21-23 September 2005, Lucerne, Switzerland.
31- K.W. Kim, Y. Park, Systematic design of tape spring hinges for solar array by optimization method considering deployment performances, Aerospace Science and Technology 46 (2015) 124–136.

32- W. Francis, M.S. Lake, K. Mallick, Development and Testing of a Hinge/Actuator Incorporating Elastic Memory Composites, Proceeding of 44th AIAA/ASME/ASCE/ AHS Structures, Structural Dynamics, and Materials Confere7-10 April 2003, Norfolk, Virginia.
33- J.W. Jeong, Y.I. Yoo, J.J. Lee, J.H. Lim, K.W. Kim, Development of a Tape Spring Hinge with a SMA Latch for a Satellite Solar Array Deployment Using the Independence Axiom, 2nd International Conference on Mechanical, Industrial, and Manufacturing Engineering. IERI Procedia 1 (2012) 225 – 231.
34- J.W. Jeong, Y.I. Yoo, D.K. Shin, J.H. Lim, K.W. Kim, J.J. Lee, A novel tape spring hinge mechanism for quasi-static deployment of a satellite deployable using shape memory alloy, Rev. Sci. Instrum. 85, 025001 (2014).
35- Xin Lan, Yanju Liu, Haibao Lv, Xiaohua Wang, Jinsong Leng and Shanyi Du, F iber reinforced shape-memory polymer composite and its application in a deployable hinge, 2009 Smart Mater. Struct. 18 024002
36- Rory Barrett, Will Francis, Erik Abrahamson, Mark Lake and Mark Scherbarth, Qualification of Elastic Memory Composite Hinges for Spaceflight Applications, 2006, 47th AIAA/ASME/ASCE/AHS/ASC Structures, Structural Dynamics and Materials Conf. (Newport, RI, May)
37- J. Choi, O.C. Kwon, W. Jo, H.J. Lee, M.W. Moon, 4D Printing Technology: A Review, 3D Printing and Additive Manufacturing, Volume 2, Number 4, 2015.
38- Stratasys, Make it more realistic and accurate with PolyJet, https://www.stratasys.com/polyjet-technology, (accessed 14 December 2020).
39- Stratasys, Data Sheet EN - VeroWhitePlus RGD835. https://support.stratasys.com/ materials/polyjet-materials/vero-family-(rigid), 2016 (accessed 14 December 2020).
40- Stratasys, Data Sheet EN - High Temperature. https://www.stratasys.com/materials/ search/high-temperature, 2018 (accessed 14 December 2020).
41- Z. Zhakypov, J.L. Huang, J. Paik, A novel torsional shape memory alloy actuator: Modeling, characterization, and control, IEEE Robotics & Automation Magazine 23.3 (2016): 65-74.
42- Isis, 6U CubeSat Platform. https://www.isispace.nl/product/6u-cubesat-platform/ (accessed 10 January 2020)
43- Gerald R. Hintz, Orbital Mechanics and Astrodynamics, Springer, 2015.
44- J. C. Ries, R. J. Eanes, C. K. Shum, M. M. Watkins, Progress in the determination of the gravitational coefficient of the Earth, Geophysical Research Letters Vol. 19, No. 6, 529-531, 1992.
45- S.M. An, J. Ryu, M. Cho, K.J. Cho, Engineering design framework for a shape memory alloy coil spring actuator using a static two-state model, Smart Materials and Structures 21 (2012) 055009.
46- S. Packirisamy, D. Schwam and M. H. Litt, Atomic oxygen resistant coatings for low earth orbit space structures, Journal of Materials Science volume 30, pages 308–320(1995), doi:10.1007/BF00354390.
47- David P. Dworak and Mark D. Soucek, Protective space coatings: a ceramer approach for nanoscale materials, Progress in Organic Coatings 47 (2003) 448–457, doi:10.1016/S0300-9440(03)00135-8.
48- Timothy K. Minton, Bohan Wu, Jianming Zhang, Ned F. Lindholm, Aziz I. Abdulagatov, Jennifer O'Patchen, Steven M. George, and Markus D. Grone, P rotecting Polymers in Space with AtomicLayer Deposition Coatings, ACS Appl. Mater. Interfaces 2010, 2, 9, 2515–2520
49- Ram K. Tripathi, John W. Wilson and Robert C. Youngquis, Electrostatic space radiation shielding, Advances in Space Research 42 (2008) 1043–1049, doi:10.1016/j.asr.2007.09.015

50- P. Spillantini, M. Casolino, M. Durante, R. Mueller-Mellin, G. Reitz, L. Rossi, V. Shurshakov and M. Sorbi, Shielding from cosmic radiation for interplanetary missions:Activeand passive methods, Radiation Measurements 42 (2007) 14–23, doi:10.1016/j.radmeas.2006.04.028.
51- Robert D. Karam, Satellite Thermal Control for Systems Engineers, American Institute of Aeronautics and Astronautics, 1998.
52- Elwood Agasid, Roland Burton, Roberto Carlino, Gregory Defouw, Andres Dono Perez, Arif Göktuğ Karacalıoğlu, Benjamin Klamm, Abraham Rademacher, James Schalkwyck, Rogan Shimmin, Julia Tilles, Sasha Weston, State of the Art Small Spacecraft Technology, NASA Ames Research Center, Small Spacecraft Systems Virtual Institute December, 2018, https://sst-soa.arc.nasa.gov/.

Appendix

A- Estimation energy collection

The estimation of the energy collection is carried out assuming a symmetric orientation of the satellite in the first and in the second half of the orbit with respect to the solar flux. Therefore, the energy collection is calculated between 0° ≤ ϑ ≤ 180° and multiplied by a factor two to account for the other half of the orbit.

A.1 Fixed panels

In the case of fixed panels, β = 0° throughout the entire orbit of the satellite. Since the panels rotate with the satellite, the solar flux has an angle of incidence $\alpha = \vartheta$ only for of half of the orbital period (see Fig. 3-a). Therefore, the energy collected by the satellite can be calculated as:

$$\boldsymbol{E_0 = \int_{-\frac{\pi}{2}}^{\frac{\pi}{2}} W_{(\vartheta)} \frac{T}{2\pi} d\vartheta = 2\int_{0}^{\frac{\pi}{2}} \Phi \cdot A_0 \cdot \cos\vartheta \cdot \varepsilon \cdot \frac{T}{2\pi} d\vartheta = \frac{1}{\pi} \cdot \Phi \cdot A_0 \cdot \varepsilon \cdot T} \qquad \text{(a-1)}$$

A.2 Sun-tracking panels

If the panels of the satellite are continuously oriented perpendicularly to the solar flux, $\beta = \vartheta$ and the energy collected is maximized. Nevertheless, this condition does not occur for the entire orbit since the active compliant hinges have a maximum angular position, which is assumed to be 90° in this calculation. Once the hinges have reached this limit position, they cannot bend further and the panels stay fixed in this position until the satellite enters in the umbra, condition that occurs in the first half orbit at ϑ_e = 108° in orbit with 40% of its period in eclipse (see Fig. 3-b). Moreover, at values of ϑ larger than 90°, the satellite would project its shadow on one of the panel, reducing the panel area exposed to the solar flux with increasing ϑ until a panel is completely darkened. Referring to Fig. A1, we calculate the reduction in panel surface exposed to the solar flux and the angle ϑ_s at which a panel is completely darkened by assuming a ratio between the length of the panel and that of the side of the satellite projecting its shadow of 2:1. The area exposed to the solar flux A_ϑ is calculated as the difference between the total area of the two panel A_0 and the panel area in the shadow A_s:

$$\boldsymbol{A_\vartheta = A_0 - A_s = 2 \cdot w \cdot l_0 - w \cdot \frac{l_0}{2} tan\left(\vartheta - \frac{\pi}{2}\right) = A_0\left(1 + \frac{1}{4}\frac{1}{tan\,\vartheta}\right)} \qquad \text{(a-2)}$$

where w is the width of the panels and l_0 the length of the side of the satellite, assumed equal to the length of the panel. The angle at which the shadow of the satellite darkens entirely a panel corresponds to the condition:

$$\frac{l_0}{2} tan\left(\vartheta - \frac{\pi}{2}\right) = l_0 \tag{a-3}$$

which return an angle ϑ_s = 153.43°. Being $\vartheta_s > \vartheta_e$, the shadow of the satellite never darkens completely a panel in the considered orbit, since the eclipse of the satellite occurs before ϑ_s is reached. Finally, the collected energy can be calculated as:

$$\begin{aligned} E_{max} &= 2\int_0^{\frac{\pi}{2}} \Phi \cdot A_0 \cdot \varepsilon \cdot \frac{T}{2\pi} d\vartheta + 2\int_{\frac{\pi}{2}}^{\frac{3\pi}{5}} \Phi A_\vartheta \cos\left(\vartheta - \frac{\pi}{2}\right) \varepsilon \frac{T}{2\pi} d\vartheta = \\ &= \frac{1}{2} \cdot \Phi \cdot A_0 \cdot \varepsilon \cdot T + \frac{\sqrt{\frac{5}{8} + \frac{\sqrt{5}}{8}} + \sqrt{5} - 2}{4\pi} \cdot \Phi \cdot A_0 \cdot \varepsilon \cdot T = \\ &= \frac{2\pi + \sqrt{\frac{5}{8} + \frac{\sqrt{5}}{8}} + \sqrt{5} - 2}{4\pi} \cdot \Phi \cdot A_0 \cdot \varepsilon \cdot T \end{aligned} \tag{a-4}$$

A.3 Three-step actuation

In the three-step actuation, the following strategy is adopted: β = 0° for 0° ≤ ϑ < 45° and β = 90° for 45° ≤ ϑ ≤ 180°. The formula (a-2) is used to correct the panel area exposed to the solar flux for ϑ > 90°. The collected energy results:

$$\begin{aligned} E_{3\,steps} &= 2\int_0^{\frac{\pi}{4}} \Phi A_0 \cos\vartheta\, \varepsilon \frac{T}{2\pi} d\vartheta + 2\int_{\frac{\pi}{4}}^{\frac{\pi}{2}} \Phi A_0 \cos\left(\vartheta - \frac{\pi}{2}\right) \varepsilon \frac{T}{2\pi} d\vartheta + \\ &+ 2\int_{\frac{\pi}{2}}^{\frac{3\pi}{5}} \Phi A_\vartheta \cos\left(\vartheta - \frac{\pi}{2}\right) \varepsilon \frac{T}{2\pi} d\vartheta = \\ &= \frac{\sqrt{2}}{2\pi} \cdot \Phi \cdot A_0 \cdot \varepsilon \cdot T + \frac{\sqrt{2}}{2\pi} \cdot \Phi \cdot A_0 \cdot \varepsilon \cdot T + \frac{\sqrt{\frac{5}{8} + \frac{\sqrt{5}}{8}} + \sqrt{5} - 2}{4\pi} \cdot \Phi \cdot A_0 \cdot \varepsilon \cdot T = \\ &= \frac{4\sqrt{2} + \sqrt{\frac{5}{8} + \frac{\sqrt{5}}{8}} + \sqrt{5} - 2}{4\pi} \cdot \Phi \cdot A_0 \cdot \varepsilon \cdot T \end{aligned} \tag{a-5}$$

A.4 Five-step actuation

In the five-step actuation, the following strategy is adopted: β = 0° for 0° ≤ ϑ < 22.5°, β = 45° for 22.5° ≤ ϑ < 67.5° and β = 90° for 67.5° ≤ ϑ ≤ 180°. The formula (a-2) is used to correct the panel area exposed to the solar flux for ϑ > 90°. The collected energy results:

$$E_{5\,steps} = 2\int_0^{\frac{\pi}{8}} \Phi A_0 \cos\vartheta\, \varepsilon \frac{T}{2\pi} d\vartheta + 2\int_{\frac{\pi}{8}}^{\frac{3\pi}{8}} \Phi A_0 \cos\left(\vartheta - \frac{\pi}{4}\right) \varepsilon \frac{T}{2\pi} d\vartheta +$$

$$+2\int_{\frac{3\pi}{8}}^{\frac{\pi}{2}} \Phi A_0 \cos\left(\vartheta - \frac{\pi}{2}\right) \varepsilon \frac{T}{2\pi} d\vartheta + 2\int_{\frac{\pi}{2}}^{\frac{3\pi}{5}} \Phi A_0 \left(1 + \frac{1}{4}\frac{1}{\tan\vartheta}\right) \sin\vartheta\, \varepsilon \frac{T}{2\pi} d\vartheta =$$

$$= \frac{\sqrt{2-\sqrt{2}}}{2\pi} \cdot \Phi \cdot A_0 \cdot \varepsilon \cdot T + \frac{\sqrt{(2-\sqrt{2})}}{\pi} \cdot \Phi \cdot A_0 \cdot \varepsilon \cdot T + \tag{a-6}$$

$$+\frac{\sqrt{2-\sqrt{2}}}{2\pi} \cdot \Phi \cdot A_0 \cdot \varepsilon \cdot T + \frac{\sqrt{\frac{5}{8} + \frac{\sqrt{5}}{8} + \sqrt{5} - 2}}{4\pi} \cdot \Phi \cdot A_0 \cdot \varepsilon \cdot T =$$

$$= \frac{8\sqrt{2-\sqrt{2}} + \sqrt{\frac{5}{8} + \frac{\sqrt{5}}{8} + \sqrt{5} - 2}}{4\pi} \cdot \Phi \cdot A_0 \cdot \varepsilon \cdot T$$

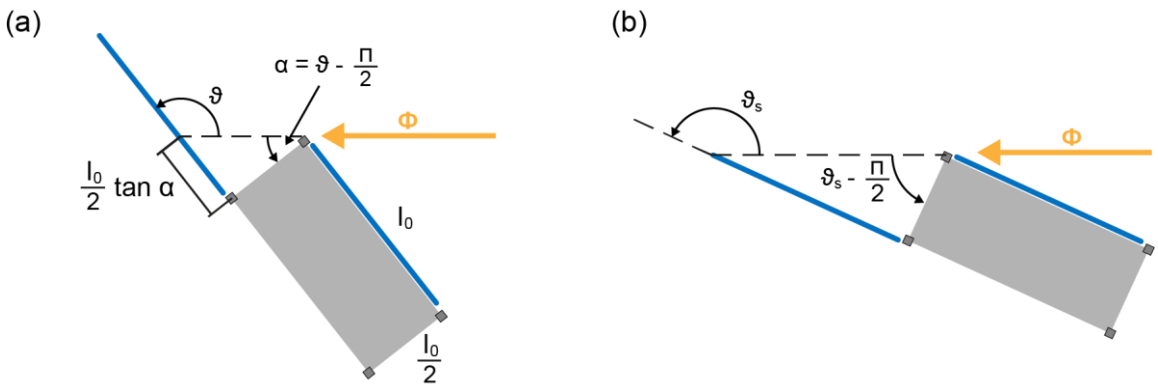

Figure A1: Orientation of the satellite (a) at $\vartheta > 90°$ and (b) at the critical angle $\vartheta = \vartheta_s$, at which one solar panel is completely darkened by the shadow of the satellite.